Applied Thermal Engineering 231 (2023) 120959

Contents lists available at ScienceDirect

Applied Thermal Engineering

journal homepage: www.elsevier.com/locate/apthermeng

Research Paper

Thermal parameters of cylindrical power batteries: Quasi-steady state heat guarding measurement and thermal management strategies

Hong Yu [a], Hengyun Zhang [a,*], Jinghe Shi [a], Shunbo Liu [a], Zhaozang Yi [a], Shen Xu [a], Xinwei Wang [b]

[a] School of Mechanical and Automotive Engineering, Shanghai University of Engineering Science, 333 Longteng Road, Songjiang, Shanghai 201620, China
[b] Department of Mechanical Engineering, 2025 Black Engineering Building, Iowa State University, Ames, IA 50011, USA

ARTICLE INFO

Keywords:
Cylindrical lithium-ion battery
Axial thermal conductivity
Specific heat
Heat guarding method
Thermal management strategies

ABSTRACT

In this work, a new quasi-steady state heat guarding measurement method for the thermophysical parameters of cylindrical batteries is proposed. The effectiveness of the heat guarding method is evaluated by the finite element analysis and the measurement of a standard ANSI 304 stainless steel sample. The heat loss is minimized to 2.4% maximum for cylindrical batteries under test based on numerical simulation. With the optimization of the test configuration, the experimental characterization of batteries was conducted to determine the thermal parameters accurately. The experimental results show that the axial thermal conductivity of 18650 and 21700 batteries are within 11.8–15.4 $W \cdot m^{-1}\,°C^{-1}$ and 12.6–16.7 $W \cdot m^{-1}\,°C^{-1}$, respectively, which are much lower than the material test values by the laser flash method. Axial thermal conductivity increases with temperature and SOC, and the specific heat increases linearly with temperature but varies little with SOC. This study demonstrates a fast, cost-effective and nondestructive way to obtain the axial thermal conductivity and specific heat of cylindrical batteries simultaneously and accurately. The subsequent thermal analysis on the thermal design of cylindrical batteries is also conducted based on the measured thermal parameters, which facilitate appropriate thermal management strategies for different types of cylindrical batteries.

1. Introduction

In recent years, electric vehicles have played an important role in mitigating energy crisis and environmental pollution, and are being developed rapidly all over the world. The lithium-ion battery has become the preferred power source for electric vehicles due to its advantages of high-power density, long lifetime and low self-discharge rate [1–3]. However, the characteristics of lithium-ion battery are closely related to the operating temperature [4–5]. When the battery temperature reaches the high threshold, the decomposition of the solid electrolyte interface layer would occur, or even worse, resulting in the battery thermal runaway accompanied with smoke, fire or explosion [6–8]. On the other hand, a low temperature leads to an increase in internal resistance and a sharp decline in the discharge capacity of battery and driving performance of electric vehicles. It was reported that capacity fade of lithium-ion battery after 600 cycles was only about 25.8% at −10 °C [9] and in extreme cases, it even prevents electric vehicles from starting directly [10–11]. Clearly, thermal management and safety of lithium-ion power batteries are becoming predominate issues in the development of electric vehicles [12–15]. To come up with optimal thermal management solutions, first and foremost, the thermophysical parameters of lithium-ion batteries in different forms are to be determined accurately, including thermal conductivity and specific heat [16]. For a typical cylindrical lithium-ion battery, the radial thermal conductivity is significantly different from the axial thermal conductivity due to the spiral roll-like structure of the anode-separator-negative material layers, together with other accessory parts and components [17].

Unfortunately, the thermophysical parameters are usually unavailable from the suppliers' specifications. There still exist discrepancies in the determination of the thermal parameters with high fidelity in literature. In many cases, the thermal conductivity is simply taken as the weighted average of the battery core layers without considering the necessary internal structure such as top and bottom insulation layers. The weighted average is mostly inaccurate due to the unconsidered factors such as the tab connection between the core materials and the terminals as well as the non-trivial contact resistances among layers

* Corresponding author.
E-mail address: zhanghengyun@sues.edu.cn (H. Zhang).

https://doi.org/10.1016/j.applthermaleng.2023.120959
Received 11 October 2022; Received in revised form 26 April 2023; Accepted 11 June 2023
Available online 16 June 2023

Nomenclature

A	the cross-sectional area channel of the cooling pipeline (m^2)
c	specific heat of battery ($J \cdot kg^{-1}\ ^\circ C^{-1}$)
c_w	specific heat of water ($J \cdot kg^{-1}\ ^\circ C^{-1}$)
F_O	thermal Fourier number
h	convective heat transfer coefficient ($W \cdot m^{-2}\ ^\circ C^{-1}$)
H	length of cylindrical battery (m)
k_r	radial thermal conductivity of battery ($W \cdot m^{-1}\ ^\circ C^{-1}$)
k_z	axial thermal conductivity of battery ($W \cdot m^{-1}\ ^\circ C^{-1}$)
q	volumetric heat generation rate of the cylinder model ($W \cdot m^{-3}$)
q''_H	heat fluxes normal to the planes Z = 0 ($W \cdot m^{-2}$)
Q_t	heat generated by the cylinder (W)
r	radial direction
R	radius (m)
$R_{r,e}$	radial equivalent thermal resistance ($^\circ C \cdot W^{-1}$)
$R_{z,e}$	axial equivalent thermal resistance ($^\circ C \cdot W^{-1}$)
S	terminal surface area of the cylindrical battery (m^2)
t	time (s)
T	temperature (°C)
T_1 T_4	measured positive and negative terminal temperatures shown in Fig. 3 (°C)
T_{amb}	environment temperature (°C)
T_{max}, T_{out}	maximum and surface temperatures of cylindrical battery respectively in Fig. 7 (°C)
T_n, T_p	average temperatures of negative terminal and positive terminals, respectively
ΔT	temperature difference between the positive and negative terminal surfaces of the battery (°C)
ΔT_r	radial temperature rise (°C)
ΔT_w	temperature rise of water (°C)
ΔT_z	axial temperature rise (°C)
ΔT_{ca}	temperature difference between the test configuration and the environment (°C)
v	velocity of flow ($m \cdot s^{-1}$)
Z	axial direction

Greek symbols

ρ	density ($kg \cdot m^{-3}$)
ρ_w	density of water ($kg \cdot m^{-3}$)

Acronym

ARC	accelerated rate calorimeter
DOE	design of experiment
DSC	differential scanning calorimetry
FEA	finite element analysis
NCM-523	$Li[Ni_{0.5}Co_{0.2}Mn_{0.3}]O_2$
NCM-811	$Li[Ni_{0.8}Co_{0.1}Mn_{0.1}]O_2$
SOC	state of charge
TCSG	thermally conductive silicone grease
HCGS	highly conductive graphite sheet

[18–19]. Maleki et al. [20] utilized the laser flash technology to measure the thermal conductivity and specific heat of the electrode material layers of the batteries, the in-plane conductivity values were measured within 29.99–39.90 $W \cdot m^{-1}\ ^\circ C^{-1}$ at 45 °C. Nonetheless, the material test at the electrode level may not be directly applicable to the battery at the cell level due to the lack of consideration of the cell structure such as tab connections with positive and negative electrode terminals.

A number of research works were devoted to develop the measurement techniques on the thermophysical parameters of lithium-ion batteries. Chen et al. [21] estimated the overall specific heat of the battery by consulting a large amount of data on the specific heat of each material that made up the battery. Villano et al. [22] tested the specific heat of each component of the battery by the method of differential scanning calorimetry (DSC) to calculate the overall specific heat by weighted average. It is noted that the above measurement methods are limited to the layered materials without considering the heterogenous structure inside the battery cells. In [23–24], the thermophysical parameters can be obtained by matching the numerical simulation results with the experimental measurements without dissection of the battery cell. Zhang et al. [23] simultaneously estimated the specific heat and thermal conductivity of large-format laminated batteries. Feng et al. [24] proposed a graphical method to determine the normal and spanwise thermal conductivity of a prismatic ternary lithium-ion battery. Nevertheless, the above methods require not only the experimental test but also the three-dimensional numerical simulation to determine thermophysical parameters, which requires long computational time and more efforts. A twin-type calorimeter was used to measure the specific heat of a cylindrical 18650 battery [25], which showed that the specific heat increased linearly with operating temperature from 20 °C to 90 °C. Bazinski et al [26] measured the specific heat of a pouch battery at different states of charge (SOC) by using an isothermal calorimeter and the specific heat was found to vary little with SOC but largely with the temperature. Efforts have also been made to obtain the thermal conductivity and specific heat simultaneously. However, the use of dedicated instruments increases the cost as well as the testing time. Sheng et al. examined the thermophysical parameters for prismatic lithium-ion batteries [27–28], in which the operating temperature had a greater effect on the specific heat of the battery than on the thermal conductivity, whereas SOC had less effect on the two parameters. Drake et al. [17] measured the thermal conductivity and specific heat of the cylindrical batteries by heating the battery from the periphery, and the 18650-type and 26650-type cylindrical lithium-ion batteries were used as experimental specimens. Anisotropic thermal conductivities were obtained with 0.20 $W \cdot m^{-1}\ ^\circ C^{-1}$ in radial direction and 30.4 $W \cdot m^{-1}\ ^\circ C^{-1}$ in axial direction for 18650 lithium-ion battery. The axial and radial specific heat results of 26650 lithium battery were 1605 $J \cdot kg^{-1}\ ^\circ C^{-1}$ and 1895 $J \cdot kg^{-1}\ ^\circ C^{-1}$, respectively, with an inconsistency of 18.1%. In another study from the same group, the radial thermal conductivity was determined to be 0.39 $W \cdot m^{-1}\ ^\circ C^{-1}$ for 26650 lithium-ion battery [29]. The heat loss along the radial heating direction was also characterized, which amounted to 50% or more, varying with the test process. As such, more efforts should be made to minimize the heat loss and improve the measurement accuracy.

The literature survey shows that some progress has been made in the measurement of thermophysical parameters but scattering in the data is still found among the different experimental studies. For cylindrical batteries, the radial thermal conductivities varied from 0.15 $W \cdot m^{-1}\ ^\circ C^{-1}$ to 3.4 $W \cdot m^{-1}\ ^\circ C^{-1}$, and the axial thermal conductivities varied from 20.06 $W \cdot m^{-1}\ ^\circ C^{-1}$ to 32.0 $W \cdot m^{-1}\ ^\circ C^{-1}$, whereas the specific heat varied from 760 $J \cdot kg^{-1}\ ^\circ C^{-1}$ to 1720 $J \cdot kg^{-1}\ ^\circ C^{-1}$ [15–16]. It is not likely that the variations in battery types and formulations in different studies could solely cause such large deviations [30]. Instead, the differences could be more attributed to the insufficient investigations on the experimental measurement methods of the battery thermophysical properties, which may lead to different levels of measurement uncertainty. Though DSC is often used to measure the specific heat of the individual materials by dissecting the battery cell [22,31], it cannot determine the average specific heat of the battery cell as a whole. The accelerated rate calorimeter (ARC) can be used to test the specific heat of a battery cell by adapting the test chamber size to the test cell, which

however is difficult to cope with the tests of realistic batteries of varying sizes. This equipment is also expensive accompanied with high operational cost and long test time [32]. Less work was conducted on the axial thermal conductivity of cylindrical battery. In the few measurements such as Drake et al. [17], single battery cells of 18650 and 26650 were used for the experimental test under quasi-steady state condition. It is important to note that the quasi-steady state measurement method is fast in obtaining the thermal parameters including thermal conductivity and specific heat. However, heat loss would accumulate to a significant portion due to the essentially low thermal conductivity and moderate heat absorption rate of a battery cell. If the heat loss is not adequately accounted for, it would lead to incorrect estimation of specific heat and thus inaccurate prediction in battery temperature and thus thermal safety state. An overestimation in the specific heat, which is typical in lack of heat loss analysis, would delay the warning time and increase the risk of premature thermal runaway [16]. Some researchers used guarded plate to measure thermal conductivity [33] to minimize the heat loss. However, development of heat guarding method for quasi-steady state measurement for battery is seldom reported. Although there were currently various methods available for measuring the thermophysical parameters of batteries, it is challenging in the validation with a standard sample of the same size and similar properties. In addition, there is insufficient reporting on the impact of operating temperature on the thermal physical performance of batteries. Therefore, the development of accurate measurement method and verification against standard samples is necessary to guarantee the measurement accuracy of battery thermal parameters.

In this work, a new quasi-steady state heat guarding measurement method for the thermophysical parameters of cylindrical batteries is proposed. In this method, the axial thermal conductivity and specific heat of the batteries can be measured in situ within a short testing time without destroying the battery. To shield the heat loss and improve the measurement accuracy, a pair of batteries was arranged at the center of the fixture socket with the negative terminal surfaces facing to each other. Multiple pairs of batteries of the same type were symmetrically arranged around the central battery pair under test to guard the unfavorable heat leaking from the lateral surfaces of the central battery pair. In this way, the lateral heat leakage was minimized to ensure one-dimensional heat flow in the axial direction and thus the axial thermal conductivity and specific heat of the cylindrical battery can be measured accurately, even if the axial length is much greater than its diameter for cylindrical batteries. The influences of the operating temperature and SOC on the thermophysical parameters of the battery were also studied. Different from previous studies [20], the heat guarding measurement can determine the axial thermal conductivity and specific heat of cylindrical batteries simultaneously in situ in a straightforward yet fast manner without dissecting the battery. In addition, the verification test of the present measurement method was also conducted based on the standard stainless-steel samples.

2. Measurement method

The schematic of a cylindrical lithium-ion battery subject to axial heating is shown in Fig. 1. For a well-designed heat guarding case as shown in Fig. 1(c), a constant heat flux q_H'' is input at the surface of $Z = H$ referred to the negative terminal surface, whereas the other boundaries are set to be adiabatic.

Subjected to the heat flux input q_H'', the temperature of the battery rises with time. According to the transient heat conduction theory [34], the quasi-steady state can be reached after a short period of heating time if all the other surfaces are adiabatic. Namely, the solid structures at the quasi-steady state have the same temperature rise rate everywhere and the temperature gradient or heat flux does not change with time. Assuming the thermal conductivity and specific heat are constant quantities given a small temperature rise range, the following equation is obtained according to energy conservation.

$$q_H'' S = mc\frac{dT}{dt} \tag{1}$$

where q_H'' is heat flux normal to the negative terminal surface of $Z = H$, S is the terminal surface area of the cylindrical battery, m and c are the mass and average specific heat of the battery, and dT/dt represents the average temperature rise rate across the battery.

Thus, the average specific heat of the battery can be expressed as

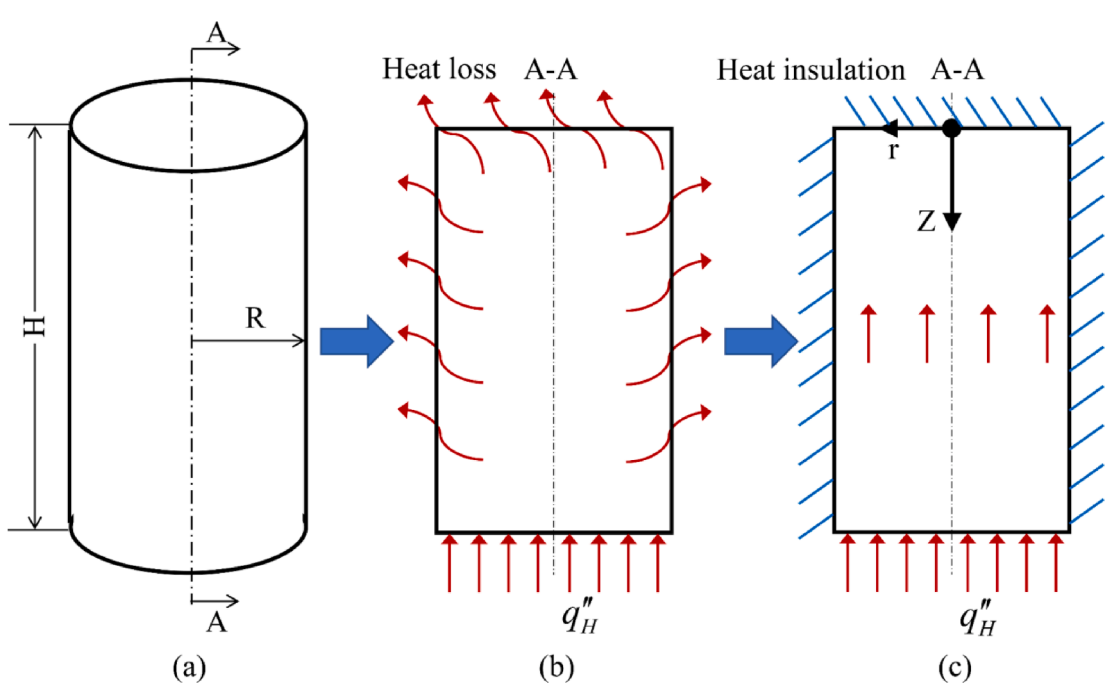

Fig. 1. Schematic of axial heating for cylindrical lithium-ion battery (a) outer dimensions, (b) actual heat flow, (c) one-dimensional axial heat conduction under adiabatic conditions.

$$c = \frac{q_H''}{\rho H \frac{dT}{dt}} \tag{2}$$

where ρ and H are density and length of the battery, respectively.

For the case of axial heating of the battery, the heat conduction differential equation and boundary conditions are given by

$$\frac{\partial^2 \theta}{\partial z^2} = \frac{\rho c}{k_z}\frac{\partial \theta}{\partial t} \tag{3}$$

$$\frac{\partial \theta}{\partial z} = \frac{1}{k_z} q_H'' \text{at } Z = H \tag{4}$$

$$\frac{\partial \theta}{\partial z} = 0 \text{at } Z = 0 \tag{5}$$

where $\theta(z,t)$ is the temperature rise, k_z is the axial thermal conductivity of the battery.

Considering that the initial temperature of the battery is same as the ambient temperature, i.e., $\theta(r,0) = 0$, the thermal differential equation (3) is solved by Laplace transform method or variable separation method, and the analytical solution of temperature field in time and space is obtained.

$$\theta(z,t) = \frac{q_H''}{\rho c H} t + \frac{q_H''}{2k_z H}\left(Z^2 - \frac{H^2}{3}\right) + \sum_{n=1}^{\infty} \frac{(-1)^{n+1} 2 q_H'' H}{k_z (n\pi)^2} cos\left(\frac{n\pi z}{H}\right) e^{(-F_O (n\pi)^2)} \tag{6}$$

where F_O is the thermal Fourier number. The thermal Fourier number is calculated during the axial conduction of the cell as follows

$$F_O = \frac{k_z t}{\rho c H^2} \tag{7}$$

According to the formula (6), an expression relating to the axial thermal conductivity k_z of the battery can be obtained by the difference between $\theta(0,t)$ and $\theta(H,t)$

$$\Delta T = -\frac{q_H'' H}{2k_z} + 2\sum_{n=1}^{\infty} \frac{(-1)^{n+1} 2 q_H'' H}{k_z (n\pi)^2} e^{(-F_O (n\pi)^2)} \tag{8}$$

where ΔT is the temperature difference between the positive and negative terminal surfaces of the battery.

The series term in Eq. (8) rapidly decays with the increase of heating time due to the exponential dependence of time. A quantitative analysis shows that the numerical value of the series terms can be ignored for F_O greater than 0.5. Therefore, the axial thermal conductivity k_z of the battery can be simplified to.

$$k_z = -\frac{q_H'' H}{2\Delta T} \tag{9}$$

It is seen that the specific heat and axial thermal conductivity can be attained based on the quasi-steady state heat transfer under the adiabatic boundary conditions with the one-dimensional axial heat conduction as shown in Fig. 1(c). Nonetheless, heat leakage becomes larger along with the heating time in the actual experimental test, especially from the large lateral surface of the cylindrical battery such as 18650 batteries, which must be minimized to ensure the measurement accuracy. In addition, the initial phase of quasi-steady state should be utilized to determine the axial thermal conductivity and the specific heat to avoid excessively high battery temperature and thus enlarged heat leakage.

In this work, the determination of the initial phase of quasi-steady state is as follows. Upon heating, the battery temperature rises quickly at the maximum rate before heat propagation to the inside. Before soon, the initial temperature rise rate is reduced to a constant level due to heat propagation to the battery core along the thermal path. In contrast, the temperature rise rate of the positive terminal surface increases steadily with the heating time from the beginning. The curves of the temperature rises and their time derivatives (temperature rise rate) of positive and negative terminal surfaces of the battery in the heating process are shown in Fig. 2. Here the average temperature of the positive terminal is denoted as $T_p = (T_1 + T_4)/2$ whereas the average of the negative terminal is $T_n = (T_2 + T_3)/2$. t_1 is denoted as the start of the initial quasi-steady state stage, at which the difference between the temperature rise rates of the positive and negative terminal is reduced within 5%. As the heating process goes on, the temperature of the battery keeps rising, and the temperature difference between the negative and positive terminal remains at the same level, indicating the quasi-state heat transfer is reached. However, the temperature difference ΔT_{ca} between the test configuration and the environment keeps increasing, which leads to more heat leakage from the test configuration to the environment. To avoid large measurement error, the initial phase of the quasi-steady state ($t_1 \sim t_2$) is set with ΔT_{ca} not more than 15 °C. In this stage, the measurement can be implemented with higher accuracy due to negligible heat leakage from the lateral surfaces to the environment, which is to be discussed in the later section.

3. Experimental

The commercial cylindrical NCM-523 18650 lithium-ion batteries supplied from LG Chemical Co., Ltd. and NCM-523 21700 lithium-ion batteries supplied from Panasonic Co., Ltd. were taken as the test batteries. The basic parameters of the battery are shown in Table 1.

3.1. Test section

The test device before and after assembly is shown in Fig. 3(a-b). The test section consisted of seven pairs of 18650 cylindrical lithium-ion batteries in a fixture socket made from 3D printing, with the pair of the batteries under test located in the center and the other six pairs

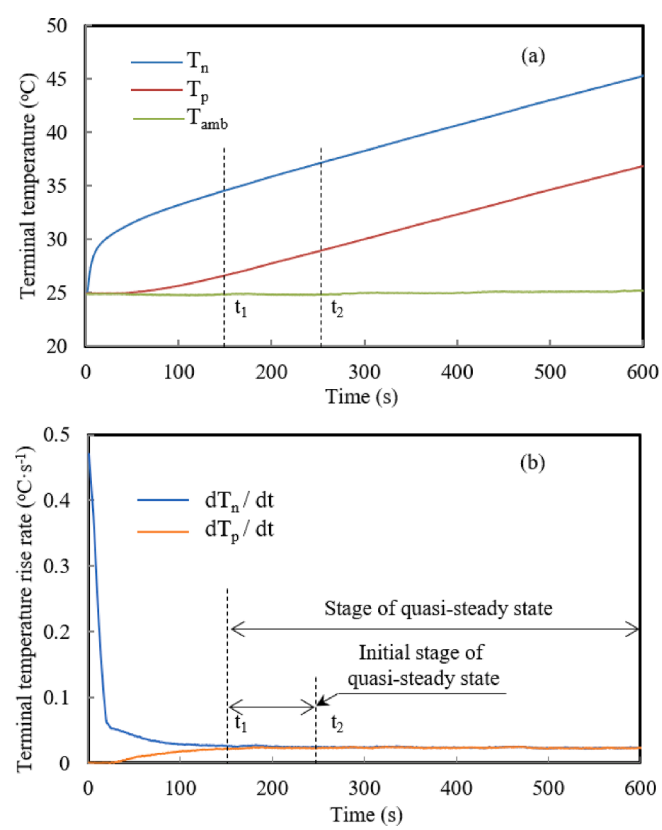

Fig. 2. (a) Temperature variations and (b) temperature rise rates for the positive and negative terminals.

Table 1
Basic parameters of the test batteries.

Parameters	18650	21700
Chemical material composition	NCM-523	NCM-523
Nominal capacity (Ah)	2.5	4.5
Nominal voltage (V)	3.6	3.7
Charge cut-off voltage (V)	4.2	4.2
Discharge cut-off voltage (V)	2.5	2.5
Max. charge current (A)	4	2
Max. discharge current (A)	30	10
Standard charge current (A)	1.25	1
Standard charge end condition (A)	0.2	0.1
Weight (g)	46	69
Length (mm)	65	70
Diameter (mm)	18.2	21.2

located evenly at the peripheral as the heat guarding batteries. Each pair of batteries of the same type was pressed end to end in between inserted with an electric heating film encapsulated with polyimide sheets. The symmetric arrangement of the two central batteries also guarantees the terminal heating without heat loss along the axial direction. Four T-type thermocouples (wire diameter of 0.1 mm, National first-class accuracy) were allocated at the two ends of the two central batteries. For each central battery, one thermocouple was fixed on the positive terminal surface (Z = 0), and the other was soldered at the lateral surface 2 mm away from the negative terminal surface (Z = 63 mm). The location of the thermocouple away from the negative electrode avoids the direct heating of the thermocouple by the heating film.

Special care must be taken to ensure the heating power to go through the battery along the axial direction. The polyimide electric heating films with a thickness of 0.14 mm, the power rating of 10 W, the applicable temperature range of −150 °C to 220 °C were selected to provide constant power heat input for the battery negative terminals, with 18 mm for 18650 battery and 21 mm for 21700 battery in diameter. A highly conductive graphite sheet with a thickness of 46 μm was attached to both ends of the heating film to homogenize the temperature of the battery. In addition, the HM-712N thermal conductive silicon grease with the thermal conductivity of 2.38 $W{\cdot}m^{-1}\ {}^{\circ}C^{-1}$ was thinly coated on the heating face of the battery, which was to reduce the contact thermal resistance with the heating film.

Two layers of 10 mm thick aerogel were wrapped around the seven pairs of batteries to reduce heat leakage and mimic an approximately adiabatic environment. The silica aerogel blanket has a thermal conductivity as low as 0.02 $W{\cdot}m^{-1}\ {}^{\circ}C^{-1}$ at 25 °C, which acts as excellent thermal insulation material to minimize the heat leakage from the large lateral side of the battery cell.

3.2. Test system

Fig. 3(d) shows the schematic diagram of the test system. It consisted of the test section, a thermostatic chamber (GDJ-250, with the accuracy of 1 °C), DC power supply (GWINSTEK GPD-2303S, with the voltage accuracy of 0.01 V, and the current accuracy of 0.001 A), temperature data acquisition equipment (AGILENT 34972A, with the uncertainty of 0.3%) and computer.

The thermocouples were fixed on the positive terminal surface and the lateral surface 2 mm away from the negative terminal surface of the two batteries under test, recorded as $T_1 \sim T_4$ in turn, which are shown in Fig. 3(d). The thermocouple to measure ambient temperature was placed at the lower end of the acrylic box to reduce the influence of air convection. The enclosed acrylic box provided a constant ambient temperature for the test section without being disturbed by the fan flow in the thermostatic chamber. The advantages of the testing system in this experiment lie in the several aspects. The test can be completed in a time period as short as several hundred seconds due to the essentially transient measurement method. The measurement accuracy is improved by one order of magnitude with the present heat guiding technique, which is to be discussed in the following section. In addition, the test equipment and materials are not difficult to implement without resorting to expensive equipment. In comparison, the ARC equipment would take several hours to obtain the specific heat due to its gradual temperature rise rate essentially requiring thermal equilibrium between the bulky chamber and the test sample [30].

3.3. Finite element analysis and method validation

The effectiveness of the heat guarding test device is visualized with the finite element analysis (FEA). Taking 18650 and 21700 lithium-ion batteries as an example, the FEA on three different test configurations as shown in Fig. 4(a-c) was conducted in ANSYS FLUENT to quantify the heat leakage and thus visualize whether the heat guarding test device is effective or not. The material parameters and boundary conditions in the numerical analysis are shown in Table 2.

Fig. 4 (d-e) shows the temperature contour plot of the battery simulation model for the test configuration with heat guarding batteries in the quasi-steady state at 600 s for 18650 and 21700 lithium-ion batteries. Although the temperature distribution in the heat guarding batteries is non-uniform due to heat leakage, good temperature uniformity is found for the central batteries. It ensures that the heat applied to the negative terminal surface of the central battery can be transferred to the positive terminal surface mainly along the axial direction. The maximum temperature difference between the central battery pair and the heat guarding batteries at the same axial position is only 0.9 °C and 1.3 °C for 18650 and 21700 lithium-ion batteries, indicating that the heat leakage from the central battery pair can be successfully prevented by the heat guarding test device.

The heat leakage rate can be numerically determined by heat flows from the lateral side of the central battery and the results are listed in Table 3 at the different temperature difference ΔT_{ca}. It is seen that the maximum proportion of the heat leakage from the lateral surface in the initial phase of the quasi-steady state is only 0.95% and 2.40% of the total heat for the test configuration for 18650 and 21700 lithium-ion batteries as given in Table 3 based on the simulation models in Fig. 4 (a). Maximum deviations occur for the single-battery configuration, in which the relative deviation is 12.98% and 18.34% for 18650 and 21700 lithium-ion batteries, respectively, one order of magnitude higher than that of the present heat guarding device. In comparison, the present heat guarding test device creates nearly adiabatic condition for the central battery pair, which avoids excessive heat leakage from the lateral surface.

The measurement method was validated for the dummy battery samples made of standard ANSI 304 stainless steel with the three test configurations, as shown in Fig. 4(a-c). The measurement results are shown in Table 4 as against the literature values in [36].

It is obvious from Table 4 that the measurement accuracy of thermal conductivity and specific heat of the test configuration with thermal insulation device is much higher than that of the other two test configurations without heat guarding batteries. In comparison, the thermal conductivity and specific heat of the single battery test configuration were overestimated by 9.45% and 30.11%, respectively. As such, it is not surprising that the thermal parameter such as the specific heat for the single battery test configuration could be obviously higher than the material test values reported in literature [20].

It is noted that the deviation of specific heat is still high up to 10.70%. After scrutinizing the test setup, the thermal interfaces between the heating film and the battery were optimized to improve the measurement accuracy by incorporating a thin layer of graphite film (46 μm) between the heating film and the batteries. The adding of the graphite film greatly enhanced the temperature uniformity of the negative terminals and further improves the measurement accuracy of specific heat.

For this purpose, the test with TCSG and HCGS was conducted for the dummy battery with a heating power of 1.19 W as against the test with TCSG only. The test was repeated three times to minimize the random

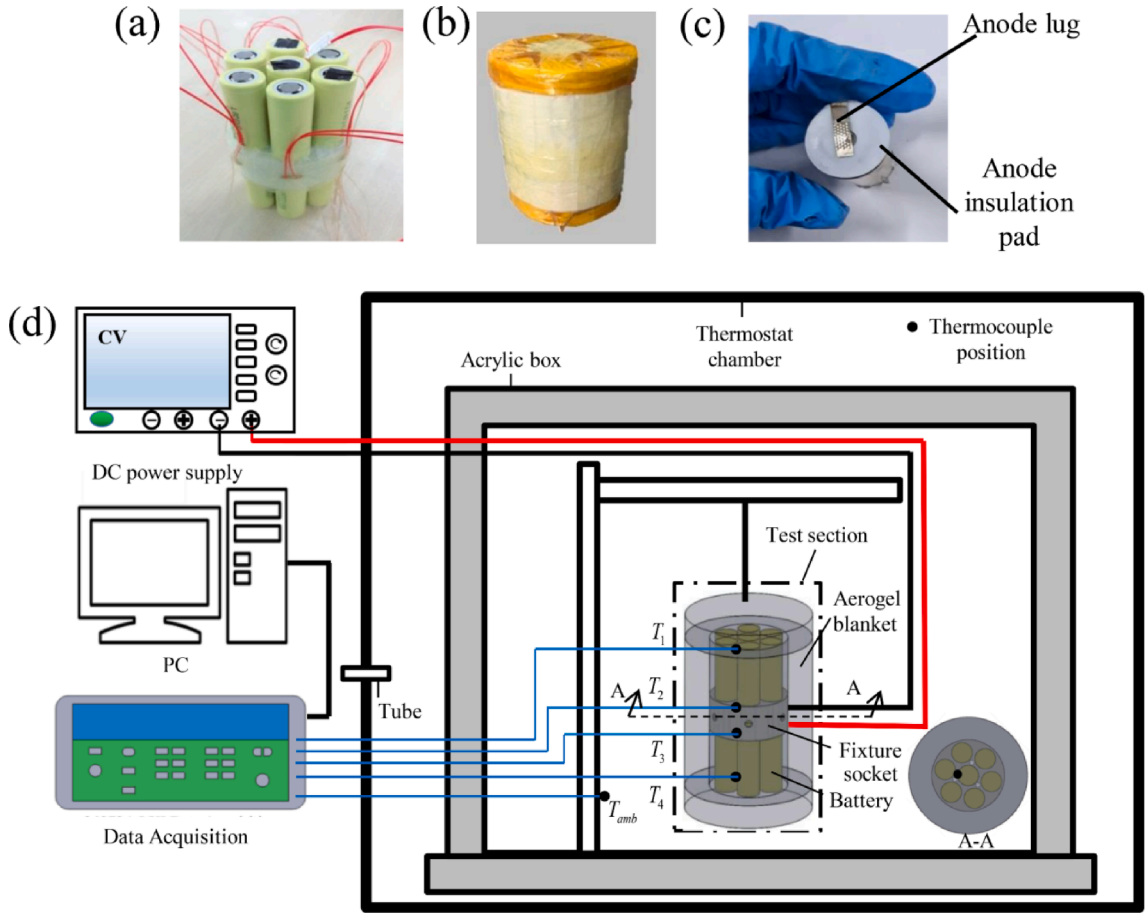

Fig. 3. Test configuration: (a) Before assembly; (b) After assembly; (c) Disassembly of battery; (d) Schematic diagram of the test system.

error due to personnel operation. The average thermal conductivity and specific heat under 25 °C of operating temperature are also tabulated in Table 4. The initial results show that the measurement errors of axial thermal conductivity and specific heat of ANSI 304 stainless steel dummy battery reached 1.01% and 10.7% with the silicone thermal grease (TCSG) only as thermal interface. With the addition of an ultra-thin layer of graphite film between the heating film and the battery, the associated measurement errors could be reduced to 0.13% and 4.99%, respectively. Clearly, the use of the ultrathin but highly conductive graphite sheet helps to homogenize the temperature at the battery bottom and thus improve the measurement accuracy.

This improvement can be explained that the TCSG may reduce the contact thermal resistance of the contact surface between the battery and the heating film, but cannot eliminate the uneven heat generation inherent in the heating film with in-built heating wire structure. When the TCSG combining with the highly conductive graphite sheet was used as the thermal interface material, the graphite sheet with a high in-plane thermal conductivity can equalize the battery temperature, reduce the fluctuation of battery temperature difference and temperature rise rate and thus improve the measurement accuracy of thermal conductivity and specific heat.

4. Results and discussion

In this section, the test results for the thermal conductivity and specific heat of cylindrical lithium-ion battery are presented and discussed. For consistency, the average thermal conductivity and specific heat capacity at the initial stage of quasi-steady state are taken as the measured values. Setting the temperature of the incubator at a fixed temperature such as 25 °C, the temperature range by the positive and negative electrodes of the battery at the initial stage of quasi-steady state is maintained within a temperature rise of 15 °C. The average temperature of positive and negative terminals is taken as the average battery operating temperature. Since both the operating temperature and SOC would affect the thermophysical parameters of the battery [35], the experimental tests of 18650 and 21700 lithium-ion batteries were carried out at four operating temperature levels (-15 °C, 5 °C, 25 °C, 45 °C) and five SOC levels (0, 0.25, 0.5, 0.75, 1) were controlled with the charge station supplied by Neware Shenzhen. The SOC level is defined at 25 °C. When testing the thermophysical parameters of batteries at different SOC levels, the 14 batteries need to be disassembled and placed separately in the tester for charging and discharging to the specified SOC. The changes of the axial thermal conductivity and specific heat of the battery in the temperature range [-4.5 °C, 55.5 °C] were investigated. It is worth noting that batteries under test were maintained at the same SOC.

4.1 Axial thermal conductivity measurement

The axial thermal conductivity of 18650 and 21700 lithium-ion batteries was measured three times using the quasi-steady state with heat guarding device and the average of the three measurements was reported. The variations of the axial thermal conductivity of the battery at different SOCs and temperatures are illustrated in Fig. 5. The results show that the axial thermal conductivity of the battery increases almost quadratically with temperature and SOC. The axial thermal conductivity of the battery mainly depends on not only the thermal conductivity of the spiral roll of the battery core with metal current collectors, active materials layers and the separator, but also the tab connection conditions between the core materials with the two terminals and interlayer

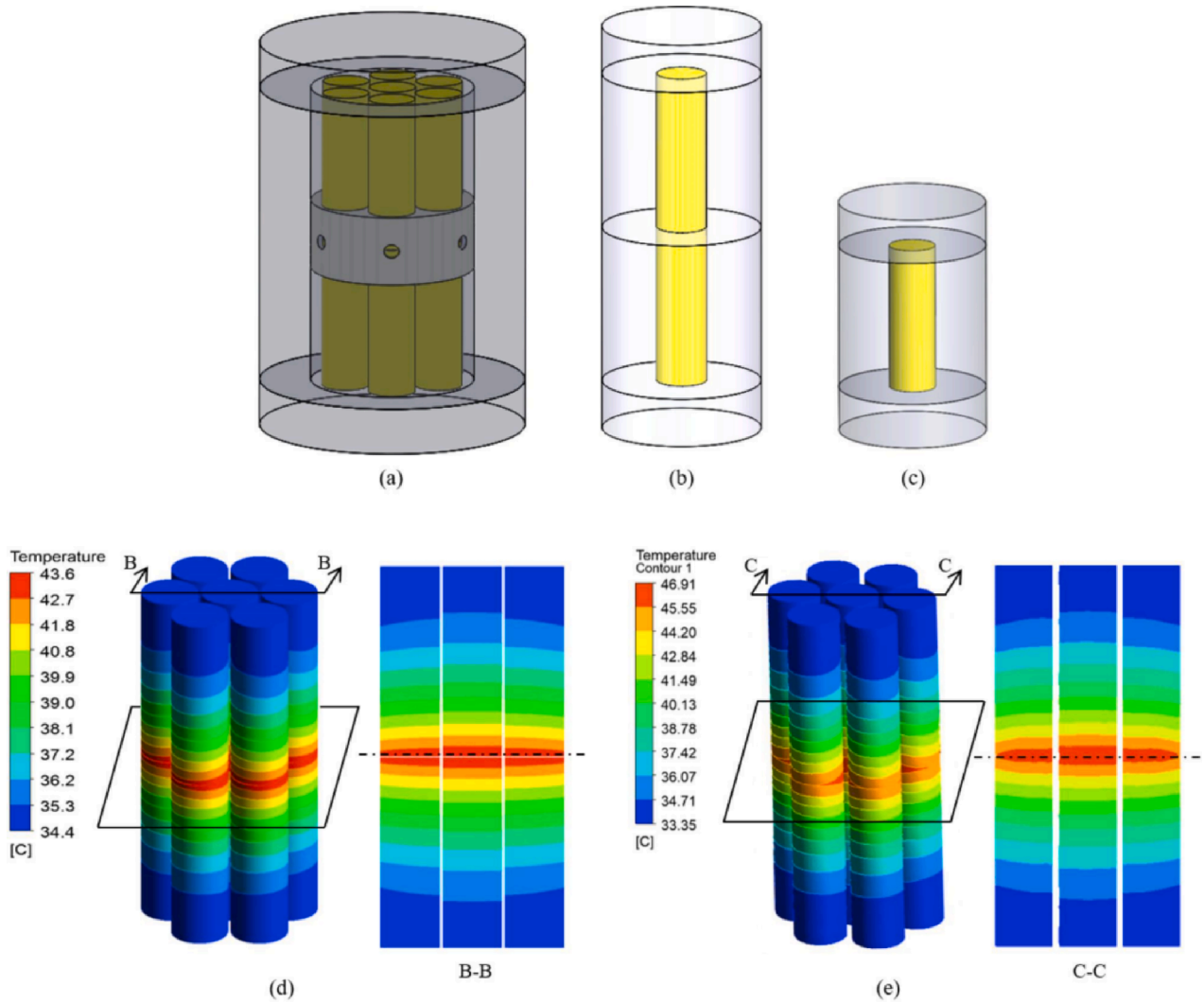

Fig. 4. Three test configurations (a) with heat guarding batteries; (b)&(c) without heat guarding batteries; (d-e) the temperature nephogram of the thermal simulation in the test configuration with heat guarding batteries for 18650 and 21700 lithium-ion batteries under heating power of 1 W and 2 W.

Table 2
The parameters in simulation model.

Parameter	Value for 18650 batteries at 25 °C	Value for 21700 batteries at 25 °C
Diameter of battery (mm)	18.2	21.2
Length of battery (mm)	65	70
Density of battery ($kg \cdot m^{-3}$)	2708	2792
Specific heat of battery ($J \cdot kg^{-1}\,°C^{-1}$)	953	1028
Axial thermal conductivity of battery ($W \cdot m^{-1}\,°C^{-1}$)	14.2 (this study)	15.2 (this study)
Radial thermal conductivity of battery ($W \cdot m^{-1}\,°C^{-1}$)	1.045 [35]	1.167 [35]
Initial temperature (°C)	25	25
h_{upper} ($W \cdot m^{-2}\,°C^{-1}$)	5	5
h_{lower} ($W \cdot m^{-2}\,°C^{-1}$)	5	5
$h_{lateral}$ ($W \cdot m^{-2}\,°C^{-1}$)	10	10
$\dot{q}_H$($W \cdot m^{-2}$)	3844	5666

Table 3
Comparison of heat leakage of three different test structures in Fig. 4.

Parameter	ΔT_{ca}(°C)	3	6	9	12	**15**
18650 batteries	Q_{loss} for Fig. 4(a)	0.09%	0.17%	0.36%	0.63%	**0.95%**
	Q_{loss} for Fig. 4(b)	2.08%	4.50%	6.47%	8.65%	**10.64%**
	Q_{loss} for Fig. 4(c)	2.85%	5.78%	8.15%	10.60%	**12.98%**
21700 batteries	Q_{loss} for Fig. 4(a)	1.81%	1.93%	2.05%	2.22%	**2.40%**
	Q_{loss} for Fig. 4(b)	2.76%	5.81%	8.18%	10.15%	**11.92%**
	Q_{loss} for Fig. 4(c)	5.93%	9.92%	12.94%	15.70%	**18.34%**

contact conditions. One of the reasons why the axial thermal conductivity increases with increasing temperature is that the thermal conductivities of the electrolytes increase with temperature rising, though the thermal conductivities of the solid compositions do not change much in such small temperature range. The thermal contact characteristics could also be improved due to the thermal expansion of solid material along the axial direction, leading to smaller contact resistance among the battery core, tab connection and the two battery terminals. On the other hand, the thermal conductivity also increases with increasing SOC, for which the negative materials intercalated with more lithium ions may expand, leading to higher internal stress and thus better thermal contact. It can also be seen from the figure that the axial thermal conductivity of 21700 lithium-ion batteries is slightly higher than that of 18650 lithium-ion batteries. This minor difference could be attributed to

Table 4
Test results and error analysis of dummy batteries made of ANSI 304 stainless steel.

Condition	ANSI 304 stainless steel	Single dummy battery		Two dummy batteries		7 pairs of dummy batteries (TCSG)		7 pairs of dummy batteries (TCSG + HCGS)	
	Standard value	Test value	Error	Test value	Error	Test value	Error	Test value	Error
Thermal conductivity ($W \cdot m^{-1}\ ^{\circ}C^{-1}$)	14.9 [36]	16.30	9.45%	15.50	4.33%	14.75	1.01%	14.92	0.13%
Specific heat ($J \cdot kg^{-1}\ ^{\circ}C^{-1}$)	477 [36]	621	30.11%	600	25.85%	528	10.70%	501	4.99%

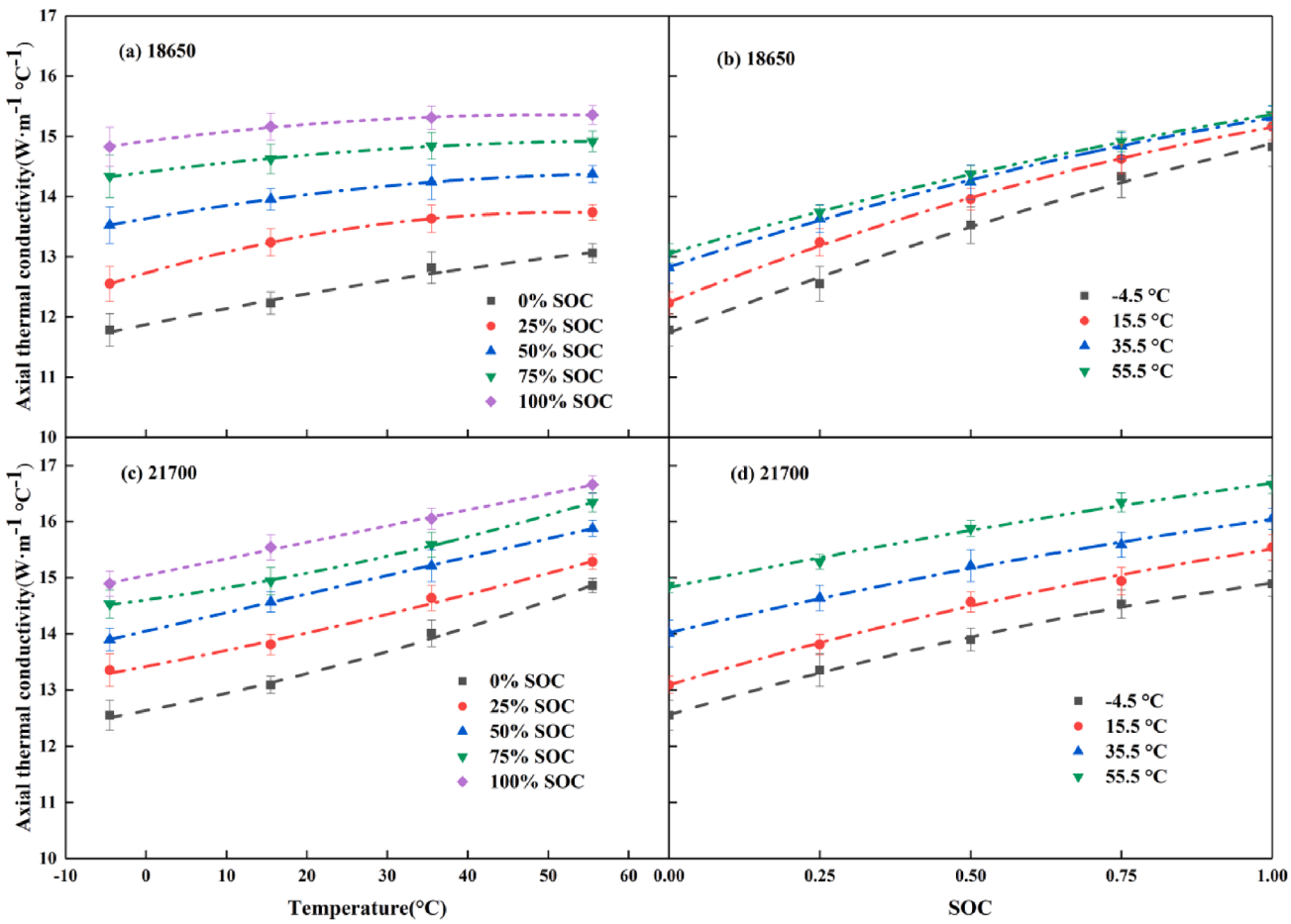

Fig. 5. Axial thermal conductivity of the 18650 and 21700 lithium-ion batteries at different SOCs and temperatures.

the differences in battery type, electrolyte, thickness of positive and negative materials, etc.

In this work, the axial thermal conductivity of 18650 lithium-ion batteries falls in between 11.8–15.4 $W \cdot m^{-1}\ ^{\circ}C^{-1}$, whereas those for 21700 lithium-ion battery fall in between 12.6–16.7 $W \cdot m^{-1}\ ^{\circ}C^{-1}$. Our battery test results are smaller than the material test values such as given in Maleki et al' work [20]. In their work, the laser flash method was used to measure the in-plane conductivity in the range of 29.99–39.90 $W \cdot m^{-1}\ ^{\circ}C^{-1}$ at 45 °C. It is noted that the large deviations between the material test and our cell test are mainly due to the additional thermal resistance associated with the tab connections with terminal metals in real battery, along with other factors such as different material compositions and structures and contact resistances among layers. In comparison, the present work is based on cell level test, which is more suitable for the realistic battery applications.

Based on the measurement results, the axial thermal conductivity of 18650 and 21700 lithium-ion batteries can be correlated into a function with respect to the temperature and SOC. Factor analysis using DOE yields the following expression.

$$k_{Z,18650} = 11.86800 + 0.032380T + 3.93578SOC - 0.014707T \times SOC - 0.000199T^2 - 0.851429SOC^2 \quad (10)$$

$$k_{Z,21700} = 12.68107 + 0.032410T + 3.04030SOC - 0.009181T \times SOC + 0.000100T^2 - 0.648496SOC^2 \quad (11)$$

The determination coefficient R^2 of 18650 and 21700 lithium-ion battery functions are 0.9976 and 0.9965 respectively. It indicates that temperature, SOC, and their second-order terms can explain 99.76% and 99.65% of the change of the axial thermal conductivity, indicating a good fitting degree of the function.

4.2. Specific heat measurement

The specific heat of the 18650 and 21700 lithium-ion batteries varies with temperature at different SOCs is illustrated in Fig. 6(a) and Fig. 6(c), respectively. The results show that the specific heat of 18650 lithium-ion batteries falls in between 884–1016 $J \cdot kg^{-1}\ ^{\circ}C^{-1}$, whereas those for 21700 lithium-ion battery fall in between 892–1082

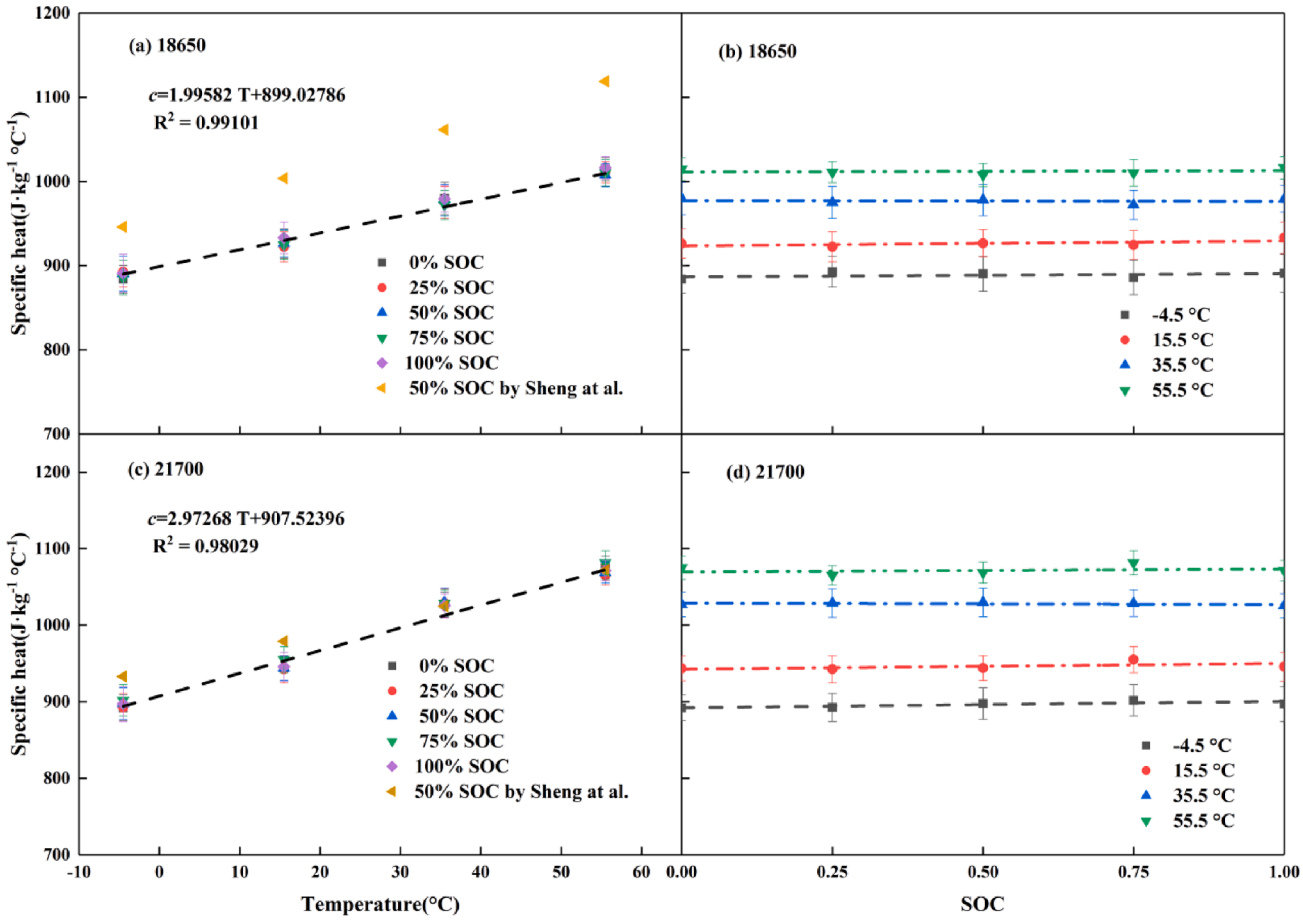

Fig. 6. Specific heat of the 18650 and 21700 lithium-ion batteries at different SOCs and temperatures in comparison with Sheng et al's data.

J·kg^{-1} °C^{-1}. The specific heat of both batteries increases linearly, with the increments of 13.18% and 19.05%, respectively, for temperature varying from −4.5 to 55.5 °C. In general, the specific heat of the solid components in the battery, including the shell, separator and current collector, increases with the increase of temperature. In addition, the molecular rotation energy, lattice vibration energy, internal energy, and electronic kinetic energy of the involved materials all increase with temperature rising, and the increase in these four energies leads to the increase structural entropy of materials. Thus, the specific heat of the battery increases with increasing temperature. This is consistent with the trend obtained in literature [31] and [37]. Loges et al. [31] measured the specific heat of six types of batteries with different materials. The results showed that the specific heat of the battery was between 870 and 1040 J·kg^{-1} °C^{-1} at 25 °C. The specific heat increased with the increase of temperature, was less affected by the state of charge (SOC), and varied with the type of battery material. Wu et al. [37] measured and investigated the specific heat of 18650 cylindrical lithium-ion batteries at different temperatures using a new calibrated calorimetric method. The results showed that the specific heat of the battery increased with increasing temperature. On the other hand, the SOC has little effect on the specific heat, as shown in Fig. 6(b) and Fig. 6(d), which is consistent with the statement in Ref. [26].

The measurement data for cylindrical 18650 batteries and 21700 batteries at 0.5 SOC by Sheng et al. [35] based on the principle of quasi-steady state heat conduction are also plotted in Fig. 6(a) and Fig. 6(c). With the similar trend in temperature, the specific heat measurement results of 18650 lithium-ion batteries in [35] are 6.28%−11.05% higher than our measurement results and those for the 21700 lithium-ion batteries are within 4% from our measurement results for the varying temperature. Such deviations could be due to different chemical compositions and manufacturing processes related to the different suppliers. Sheng et al. [35] used NCM-811 cylindrical 18650 lithium-ion battery and NCM-523 21700 lithium-ion battery supplied from Shenzhen BAK BATTERY Co., Ltd. In comparison, the test batteries in our study are the NCM-523 18650 lithium-ion batteries from LG Chemical Co., Ltd. and NCM-523 21700 lithium-ion batteries from Panasonic Co., Ltd.

Based on the measurement results, the function between specific heat of the 18650 and 21700 lithium-ion batteries and the temperature was fitted by the least square technique dependent on temperature.

$$c_{18650} = 899.02786 + 1.99582\,T \tag{12}$$

$$c_{21700} = 907.52396 + 2.97268\,T \tag{13}$$

The determination coefficient R^2 of this function is 0.99101 and 0.98029, indicating a good fitting degree for the specific heat.

4.3. Comparison with the existing test methods in literature

The present heat guarding method is also compared with existing measurement methods on thermophysical parameters of batteries. As listed in Table 5, both the c and axial thermal conductivity k_z parameters simultaneously can be measured by the present heat guarding method in a shortest measurement time. In addition, the operating temperature range of the heat guarding method is wider than that of the other test methods of the published work, which caters for the application scenarios. In a word, the present heat guarding method has the advantages of accurate and fast measurement of both specific heat and thermal conductivity without resorting to expensive equipment, which is a novel work in the battery thermal characterization and thermal management

Table 5
Comparison with the published work on thermophysical parameters of batteries.

Source	Battery type	Test method	Operating temperature measurement	Test time	Multiple parameters at the same time?
Drake [17]	18650 and 26650 cells	Quasi-steady state measurement	25 °C	1000 s	Yes (c and thermal conductivity)
Maleki [20]	pouch cells	DSC (The battery needs to be disassembled)	45 °C	60 s	No (only c)
Zhang [23]	large-format laminated cells	Simultaneous estimation (needs to compare with simulation)	25 °C	3000 s	Yes (c, thermal conductivity and thermal conductance)
Muhammad [29]	26650 cells	Time-varying heat flux method	room temperature	2100 s	No (only k_r)
Wang [32]	18650 cells	ARC	25 °C–45 °C	80 min	No (c and heat generation measured separately)
This work	18650 and 21700 cells	Heat guarding measurement method	−15 °C to 45 °C	~600 s	Yes (c and k_z)

design.

4.4. Analysis of thermal management strategies

The axial thermal conductivity would have a significant impact on the thermal management strategies of the cylindrical battery, which is analyzed in this section. Fig. 7(a) shows a homogeneous cylinder with heat production rate q, length H, radius R and cross-sectional area S, and the heat generated by the cylinder is Q_t. The thermal management can be implemented either in the axial direction with bottom cooling channels such as the design for Rivian EV battery pack [38] or in radial direction with serpentine cooling channels such as the design for Tesla EV battery pack [39]. The present heat transfer analysis is to demonstrate the dependence of thermal design on the axial thermal conductivity of the cylinder. In realistic assembly, there exist air gaps or structural glues between battery cells, which have much lower thermal conductivity and thus the cell-to-cell heat conduction is thus not considered for both lateral cooling and bottom cooling. Due to the small amount of heat generation of the battery cell under normal operation, the temperature distribution along the high-performance cold plate is not considered.

For bottom cooling in Ref. [40], we assumed $v = 1$ m/s coolant, according to the energy balance equation.

$$\Delta T_w = \frac{Q_t}{\rho_w A v c_w} \tag{14}$$

where ΔT_w is water temperature rise, ρ_w is density of water, A is the cross-sectional area channel of the cooling pipeline, c_w is the specific heat of water. A calculation shows that the fluid temperature increases by 0.049 °C for the battery cell operated at 2.5C (1.39 W) [40], which is negligible for the present cell level analysis.

According to heat transfer analysis, the maximum temperature rises of ΔT_z for the bottom cooling along with axial heat transfer occurs at the top surface as shown in Fig. 7(a), whereas the maximum temperature rises of ΔT_r along with radial heat transfer occurs at the center line of the battery.

For the bottom cooling, the maximum temperature rise is obtained as [41]

$$\Delta T_z = T_{max} - T_{out} = \frac{1}{2}\frac{H}{k_z S} Q_t = Q_t R_{z,e} \tag{15}$$

For the lateral cooling typically with serpentine tubes, the maximum temperature rise is given as

$$\Delta T_r = T_{max} - T_{out} = \frac{Q_t}{4\pi k_r H} = Q_t R_{r,e} \tag{16}$$

The equivalent axial and radial equivalent thermal resistances, defined by the ratio of the temperature difference to the heat flow, can be expressed in term of geometrical dimensions and material properties, namely.

$$R_{z,e} = \frac{1}{2}\frac{H}{k_z S} \tag{17}$$

$$R_{r,e} = \frac{1}{4\pi k_r H} \tag{18}$$

Dividing Eq. (16) by Eq. (15), the ratio of the maximum temperature rises based on radial cooling and bottom cooling is obtained as follows

$$\frac{\Delta T_r}{\Delta T_z} = \frac{R_{r,e}}{R_{z,e}} = \frac{k_z R^2}{2 k_r H^2} \tag{19}$$

When the ratio $\frac{\Delta T_r}{\Delta T_z} > 1$, the axial thermal resistance is smaller and thus the bottom cooling is preferred to reduce the maximum temperature . Vice versa, a lateral side cooling is preferred for $\frac{\Delta T_r}{\Delta T_z} < 1$ to reduce the maximum temperature of the cylindrical battery.

The curves of the maximum temperature rise ratio of radial and axial direction for different types of batteries with the ratio of axial and radial thermal conductivity are drawn in Fig. 8. Note that the radial thermal conductivity by Sheng et al. [35] has been adopted to perform the thermal design analysis for the present 18650 and 21700 batteries.

It can be seen from Fig. 8 that, at the ratio of axial and radial thermal conductivity is less than 104 for 18650 lithium-ion batteries, $\frac{\Delta T_r}{\Delta T_z} < 1$ and thus a lateral side cooling effect is better than the bottom cooling. For 21700 lithium-ion batteries, a lateral side cooling effect is better at the ratio of axial and radial thermal conductivity is less than 89. For the present 18650 and 21700 batteries measured axial thermal conductivity, the temperature rise ratios are both less than one and thus it can be concluded that the lateral side cooling is applicable for both types of batteries.

The 46800 lithium-ion battery with full-tab design is identified to be one of the next-generation high power batteries for vehicle application [42], which is also analyzed here. However, the battery is not available in the market. To facilitate the analysis, we assumed the k_r of 46800 batteries is the same as 21700 lithium-ion batteries measured by Sheng et al. [35], whereas the axial thermal conductivity is the same as the material test values by Maleki et al. [20] since their measurement was focused on the battery material which is more conformable to the 46800 lithium-ion battery with full-tab design, avoiding the high thermal resistance associated with the single tab connection for conventional cylindrical batteries. The temperature difference ratio of 46800 batteries with assumed thermal conductivity vs the ratio of k_z and k_r is shown in Fig. 8. It is seen that the ratio of ΔT_r over ΔT_z is larger than one, indicating a bottom cooling is preferred for the new 46800 battery. It should be noted that the present thermal management is a preliminary analysis with measured battery thermal parameters through the simplified thermal resistance network at the cell level. More careful analysis of thermal management in full scale could be conducive in the next stage work.

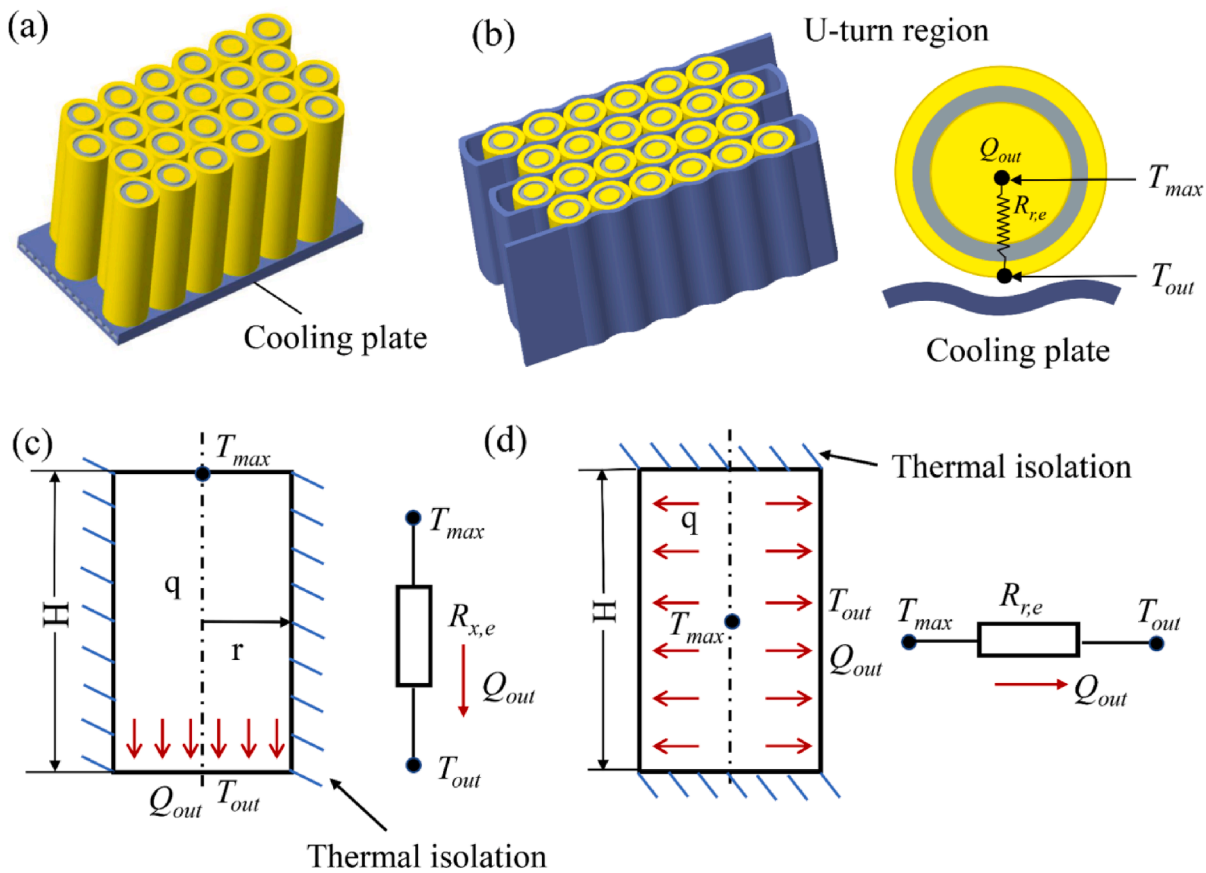

Fig. 7. (a) bottom cooling; (b) axial cooling with curved tube; (c) the size parameter, boundary condition and equivalent thermal resistance along the axial direction; (d) heat conduction model with equivalent thermal resistance along the radial direction.

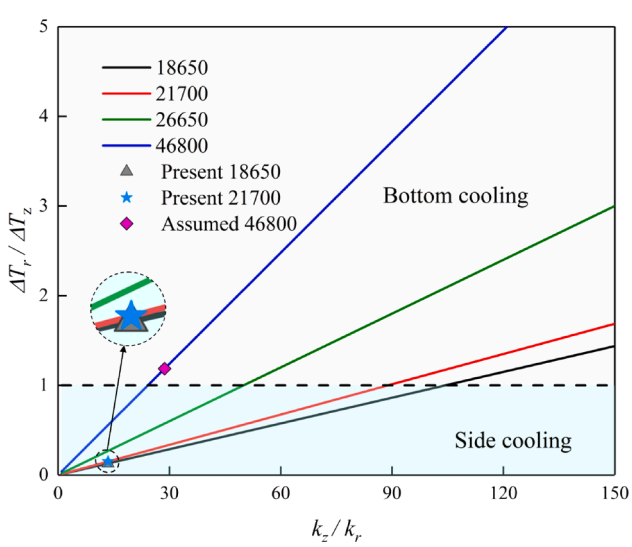

Fig. 8. Variations of the maximum temperature rise ratio with the axial and radial thermal conductivity ratio for different types of batteries.

4.5. Experimental uncertainty analysis

The test uncertainty of the axial thermal conductivity and specific heat of the battery can be attributed to the inaccuracy of test equipment, the random error associated with the dimension's temperatures measured with thermocouples, and some human factors caused by the operation.

In this work, the uncertainty of T-type thermocouple with level one accuracy is estimated to be 1% considering the temperature accuracy of 0.1 °C within 10 °C temperature range. The uncertainty of Agilent data acquisition instrument, vernier caliper and electronic balance is 0.3%, 0.1% and 1%, respectively. In addition, the accuracy of the voltage and current of the DC supply is 0.01 V and 0.001 A, respectively, and thus the uncertainty of the heating power is about 0.3%. The uncertainty caused by specific experimental instruments in each experiment is shown in Table 6.

Summing the uncertainty of experimental equipment and the random error, the uncertainties of 18650 battery, the heat flux ($\frac{\Delta \ddot{q}_H}{q_H}$), density ($\frac{\Delta \rho}{\rho}$), length ($\frac{\Delta H}{H}$) and temperature ($\frac{\Delta T}{T}$) are obtained, which are 1.64%, 1.13%, 0.23% and 2.60%, respectively. The uncertainties of 21700 battery, heat flux ($\frac{\Delta \ddot{q}_H}{q_H}$), density ($\frac{\Delta \rho}{\rho}$), length ($\frac{\Delta H}{H}$) and temperature ($\frac{\Delta T}{T}$) are 1.96%, 1.12%, 0.22% and 2.60%, respectively.

According to the root-sum-square technique [43], the uncertainties of the axial thermal conductivity and specific heat of the battery can be calculated by the following equations.

Table 6
Uncertainty analysis of experimental instruments.

Experimental instrument	Accuracy	Uncertainty
Thermocouple	National first-class accuracy	1%
Agilent data acquisition instrument	0.3%	0.3%
Vernier caliper	0.1%	0.1%
Electronic balance	1%	1.0%
DC supply	0.01 V, 0.001 A	1.0%

$$\frac{\Delta c}{c} = \sqrt{\left(\frac{\Delta q_H''}{q_H''}\right)^2 + \left(\frac{\Delta \rho}{\rho}\right)^2 + \left(\frac{\Delta H}{H}\right)^2 + \left(\frac{\Delta T}{T}\right)^2} \tag{20}$$

$$\frac{\Delta k_z}{k_z} = \sqrt{\left(\frac{\Delta q_H''}{q_H''}\right)^2 + \left(\frac{\Delta H}{H}\right)^2 + \left(\frac{\Delta T}{T}\right)^2} \tag{21}$$

The uncertainty of the axial thermal conductivity k_z and specific heat c is approximately 3.1% and 3.3% maximum for the 18650 lithium-ion batteries and 3.3% and 3.5% for the 21700 lithium-ion batteries respectively by plus the random error due to personel assembly and operation.

5. Conclusions

A novel quasi-steady state heat guarding measurement method is proposed for measuring the axial thermal conductivity and specific heat of cylindrical battery based on the principle of quasi-steady state heat conduction. The axial thermal conductivity and specific heat of 18650 and 21700 cylindrical lithium-ion batteries with large a length to diameter ratio were measured at different levels of temperature and SOC. This method has the advantages of fast, cost-effective easy operation and nondestructive, and can obtain the axial thermal conductivity and specific heat of cylindrical batteries simultaneously and accurately. In addition, the impact of the axial thermal conductivity on thermal management strategies for different batteries is analyzed and discussed.

The experimental results show that the axial thermal conductivity of 18650 and 21700 battery are within 11.8–15.4 $W{\cdot}m^{-1}\ {}^{\circ}C^{-1}$ and 12.6–16.7 $W{\cdot}m^{-1}\ {}^{\circ}C^{-1}$, respectively, whereas those for specific heat are within 884–1016 $J{\cdot}kg^{-1}\ {}^{\circ}C^{-1}$ and 892–1082 $J{\cdot}kg^{-1}\ {}^{\circ}C^{-1}$, respectively. Axial thermal conductivity of the battery increases almost quadratically with temperature and SOC, whereas specific heat increases linearly with temperature but varied little with SOC.

The numerical simulation and experimental results show that the heat guarding measurement method composed of guarding batteries possesses an excellent thermal shielding effect. The heat leakage can be minimized to 2.4% in the initial phase of the quasi-steady state based on the finite element analysis, which was one order of magnitude less than the single battery test configuration without heat guarding batteries. The maximum temperature difference between the central battery pair and the heat guarding batteries was experimentally identified to be around 1.3 °C at the same height along the battery axis.

Experimental results show that the axial thermal conductivity of the lithium-ion battery increases almost quadratically with battery temperature and SOC. The specific heat of the lithium-ion battery increases linearly with the increase of battery temperature, which remains almost unchanged at different SOCs. The presently obtained data are useful in the design and optimization of battery thermal management system. Equivalent thermal resistance analysis is conducted to assess the effectiveness of bottom cooling and lateral side cooling techniques for different types of cylindrical batteries. The results show that the lateral side cooling is more suitable for the present slim 18650 and 21700 lithium-ion batteries. For the new-type 46800 lithium-ion battery with assumed thermal conductivity, the bottom cooling is recommended instead as the optimal cooling configuration.

CRediT authorship contribution statement

Hong Yu: Methodology, Investigation, Formal analysis, Writing – original draft, Visualization. **Hengyun Zhang:** Conceptualization, Resources, Supervision, Validation, Writing – review & editing, Funding acquisition, Project administration. **Jinghe Shi:** Data curation, Investigation. **Shunbo Liu:** Writing – review & editing, Supervision. **Zhaozang Yi:** Writing – review & editing. **Shen Xu:** Data curation, Investigation. **Xinwei Wang:** Data curation, Investigation.

Declaration of Competing Interest

The authors declare that they have no known competing financial interests or personal relationships that could have appeared to influence the work reported in this paper.

Data availability

Data will be made available on request.

Acknowledgement

Financial supports from Shanghai Municipal Natural Science Foundation (21ZR1426300) and Natural Science Foundation of China (51876113) are acknowledged.

References

[1] X.T. Liu, Z.H. Chen, C.B. Zhang, J. Wu, A novel temperature-compensated model for power Li-ion batteries with dual-particle-filter state of charge estimation, Appl. Energy 123 (2014) 263–272, https://doi.org/10.1016/j.apenergy.2014.02.072.
[2] S.S.Y. Ng, Y.J. Xing, K.L. Tsui, A naive Bayes model for robust remaining useful life prediction of lithium-ion battery, Appl. Energy 118 (2014) 114–123, https://doi.org/10.1016/j.apenergy.2013.12.020.
[3] M. Mathew, Q.H. Kong, J. McGrory, M. Fowler, Simulation of lithium-ion battery replacement in a battery pack for application in electric vehicles, J. Power Sources 349 (2017) 94–104, https://doi.org/10.1016/j.jpowsour.2017.03.010.
[4] Z. Lu, X.L. Yu, L.C. Wei, F. Cao, L.Y. Zhang, X.Z. Meng, L.W. Jin, A comprehensive experimental study on temperature-dependent performance of lithium-ion battery, Appl. Therm. Eng. 158 (2019), 113800, https://doi.org/10.1016/j.applthermaleng.2019.113800.
[5] S. Ma, M. Jiang, P. Tao, C. Song, J. Wu, J. Wang, T. Deng, W. Shang, Temperature effect and thermal impact in lithium-ion batteries: A review, Prog. Nat. Sci.: Mater. Int. 28 (6) (2018) 653–666.
[6] Q.S. Wang, P. Ping, X.J. Zhao, G.Q. Chu, J.H. Sun, C.H. Chen, Thermal runaway caused fire and explosion of lithium-ion battery, J. Power Sources 208 (2012) 210–224, https://doi.org/10.1016/j.jpowsour.2012.02.038.
[7] Z.C. Feng, Y.W. Zhang, Safety monitoring of exothermic reactions using time derivatives of temperature sensors, Appl. Therm. Eng. 66 (2014) 346–354, https://doi.org/10.1016/j.applthermaleng.2014.02.023.
[8] X. Feng, D. Ren, X. He, M. Ouyang, Mitigating Thermal Runaway of Lithium-Ion Batteries, Joule 4 (2020) 743–770, https://doi.org/10.1016/j.joule.2020.02.010.
[9] Y.C. Zhang, C.Y. Wang, X.D. Tang, Cycling degradation of an automotive LiFePO4 lithium-ion battery, J. Power Sources 196 (2011) 1513–1520, https://doi.org/10.1016/j.jpowsour.2010.08.070.
[10] C.K. Huang, J.S. Sakamoto, J. Wolfenstine, S. Surampudi, The Limits of Low-Temperature Performance of Li-ion Cells, J. Electrochem. Soc. 147 (2000) 2893–2896, https://doi.org/10.1149/1.1393622.
[11] Z.Y. Ling, X.Y. Wen, Z.G. Zhang, X.M. Fang, X.N. Gao, Thermal management performance of phase change materials with different thermal conductivities for Li-ion battery packs operated at low temperatures, Energy 144 (2018) 977–983, https://doi.org/10.1016/j.energy.2017.12.098.
[12] Y.Y. Liu, Y.Y. Zhu, Y. Cui, Challenges and opportunities towards fast-charging battery materials, Nat. Energy 4 (2019) 540–550, https://doi.org/10.1038/s41560-019-0405-3.
[13] Z.H. Rao, S.F. Wang, A review of power battery thermal energy management, Renew. Sustainable Energy Rev. 15 (2011) 4554–4571, https://doi.org/10.1016/j.rser.2011.07.096.
[14] H. Jouhara, N. Khordehgah, N. Serey, S. Almahmoud, S.P. Lester, D. Machen, L. Wrobel, Applications and thermal management of rechargeable batteries for industrial applications, Energy 170 (2019) 849–861.
[15] G. Offer, Y. Patel, A. Hales, L.B. Diza, M. Marzook, Cool metric for lithium-ion batteries could spur progress, Nature 582 (2020) 485–487, https://doi.org/10.1038/d41586-020-01813-8.
[16] Y. Zeng, D. Chalise, S.D. Lubner, S. Kaur, R.S. Prasher, A review of thermal physics and management inside lithium-ion batteries for high energy density and fast charging, Energy Storage Mater. 41 (2021) 264–288.
[17] S.J. Drake, D.A. Wetz, J.K. Osanek, S.P. Miller, J.M. Heinzel, A. Jain, Measurement of anisotropic thermophysical properties of cylindrical Li-ion cells, J. Power Sources 252 (2014) 298–304, https://doi.org/10.1016/j.jpowsour.2013.11.107.
[18] R. Ponnappan, T.S. Ravigururajan, Contact thermal resistance of Li-ion cell electrode stack, J. Power Sources 129 (2004) 7–13, https://doi.org/10.1016/j.jpowsour.2003.11.006.
[19] Y. Yang, X.P. Huang, Z.Y. Cao, G. Chen, Thermally conductive separator with hierarchical nano/microstructures for improving thermal management of batteries, Nano Energy 22 (2016) 301–309, https://doi.org/10.1016/j.nanoen.2016.01.026.
[20] H. Maleki, H. Wang, W. Porter, J. Hallmark, Li-ion polymer cells thermal property changes as a function of cycle-life, J. Power Sources 263 (2014) 223–230, https://doi.org/10.1016/j.jpowsour.2014.04.033.

[21] S.C. Chen, C.C. Wan, Y.Y. Wang, Thermal analysis of lithium-ion batteries, J. Power Sources 140 (2005) 111–124, https://doi.org/10.1016/j.jpowsour.2004.05.064.
[22] P. Villano, M. Carewska, S. Passerini, Specific heatacity of lithium polymer battery components, Thermochim. Acta 402 (2003) 219–224, https://doi.org/10.1016/S0040-6031(02)00612-3.
[23] J.B. Zhang, B. Wu, Z. Li, J. Huang, Simultaneous estimation of thermal parameters for large-format laminated lithium-ion batteries, J. Power Sources 259 (2014) 106–116, https://doi.org/10.1016/j.jpowsour.2014.02.079.
[24] X.N. Feng, J.J. Li, L. Wang, J. Gao, X.M. He, M.G. Ouyang, Experiments and modeling of anisotropic thermal conductivity of lithium-ion batteries, J. Automotive Safety and Energy 3 (2012) 158–164, https://doi.org/10.3969/j.issn.1674-8484.2012.01.009.
[25] K. Onda, T. Ohshima, M. Nakayama, K. Fukuda, T. Araki, Thermal behavior of small lithium-ion battery during rapid charge and discharge cycles, J. Power Sources 158 (2006) 535–542, https://doi.org/10.1016/j.jpowsour.2005.08.049.
[26] S.J. Bazinski, X. Wang, Experimental study on the influence of temperature and state-of-charge on the thermophysical properties of an LFP pouch cell, J. Power Sources 293 (2015) 283–291, https://doi.org/10.1016/j.jpowsour.2015.05.084.
[27] L. Sheng, L. Su, H.Y. Zhang, Y.D. Fang, H.F. Xu, W. Ye, An improved calorimetric method for characterizations of the specific heat and the heat generation rate in a prismatic lithium ion battery cell, Energy Convers. Manage. 180 (2019) 724–732, https://doi.org/10.1016/j.enconman.2018.11.030.
[28] L. Sheng, L. Su, H.Y. Zhang, Experimental determination on thermal parameters of prismatic lithium ion battery cells, Int. J. Heat Mass Transfer 139 (2019) 231–239, https://doi.org/10.1016/j.ijheatmasstransfer.2019.04.143.
[29] M.B. Ahmed, S. Shaik, A. Jain, Measurement of radial thermal conductivity of a cylinder using a time-varying heat flux method, Int. J. Heat Mass Transfer 129 (2018) 301–308, https://doi.org/10.1016/j.ijthermalsci.2018.03.008.
[30] F. Richter, S. Kjelstrup, P.J.S. Vie, S.O. Burheim, Thermal conductivity and internal temperature profiles of Li-ion secondary batteries, J. Power Sources 359 (2017) 592–600, https://doi.org/10.1016/j.jpowsour.2017.05.045.
[31] A. Loges, S. Herberger, P. Seegert, T. Wetzel, A study on specific heat capacities of Li-ion cell components and their influence on thermal management, J. Power Sources 336 (2016) 341–350, https://doi.org/10.1016/j.jpowsour.2016.10.049.
[32] L. Wang, X.N. Feng, G. Xue, etc. ARC experimental and data analysis for safety evaluation of Li-ion batteries, Energy Storage Sci. Technol. 7(2018): 1261-1270. 10.12028/j.issn.2095-4239.2018.0161.
[33] A. Palacios, L. Cong, M.E. Navarro, Y.L. Ding, C. Barreneche, Thermal conductivity measurement techniques for characterizing thermal energy storage materials-A review, Renew. Sustainable Energy Rev. 108 (2019) 32–52, https://doi.org/10.1016/j.rser.2019.03.020.
[34] H.P. Hu, On the Conditions Necessary and Sufficient for Establishing Quasistationary Temperature Distribution, J. Appl. Sci. 22 (2004) 91–93.
[35] L. Sheng, Z.D. Zhang, L. Su, H.Y. Zhang, H. Zhang, Y.D. Fang, K. Li, W. Ye, Quasi steady state method to measure thermophysical parameters of cylindrical lithium ion batteries, J. Power Sources 485 (2021), 229342, https://doi.org/10.1016/j.jpowsour.2020.229342.
[36] F.P. Incropera, D.P. DeWitt, T.L. Bergeman, Fundamentals of Heat and Mass Transfer, sixth ed., John Wiley & Sons Inc, 2007.
[37] Q.Y. Wu, H.Y. Zhang, J.W. Li, Calibrated Calorimetry for Measuring the Specific heat and Heat Generation Rate of Lithium-ion Battery, Automot. Eng. 42 (2020) 59-65, 10.19562/j.chinasae.qcgc.2020.01.009.
[38] J. King, Electric vehicle thermal management system with battery heat storage, U. S Patent 15, 716, 333[P]. 2018-3-29. https://patents.google.com/patent/US20180086224A1/en.
[39] C.R. Zhao, W.J. Cao, T. Dong, F.M. Jiang, Thermal behavior study of discharging/charging cylindrical lithium-ion battery module cooled by channeled liquid flow, Int. J. Heat Mass Transfer 120 (2018) 751–762, https://doi.org/10.1016/j.ijheatmasstransfer. 2017.12.083.
[40] H.Y. Zhang, X.Y. Wu, Q.Y. Wu, S. Xu, Experimental investigation of thermal performance of large-sized battery module using hybrid PCM and bottom liquid cooling configuration, Appl. Therm. Eng. 159 (2019), 113968, https://doi.org/10.1016/j.applthermaleng.2019.113968.
[41] J.J. Zhu, H.Y. Zhang, G.P. Wu, S.L. Zhu, W. Liu, Thermal performance of cylindrical battery module with both axial and radial thermal paths: Numerical simulation and thermal resistance network analysis, J. Energy Storage 49 (2022), 104197, https://doi.org/10.1016/j.est.2022.104197.
[42] T.G. Tranter, R. Timms, P.R. Shearing, D.J.L. Brett, Communication—Prediction of thermal issues for larger format 46800 cylindrical cells and their mitigation with enhanced current collection, J. Electrochem. Soc. 167 (2020), 160544, https://doi.org/10.1149/1945-7111/abd44f.
[43] R.J. Moffat, Describing the uncertainties in experimental results, Exp. Therm. Fluid Sci. 1 (1988) 3–17, https://doi.org/10.1016/0894-1777(88)90043-X.